Lab on a Chip

Micro- & nano- fluidic research for chemistry, physics, biology, & bioengineering

www.rsc.org/loc

Volume 10 | Number 4 | 21 February 2010 | Pages 397–528

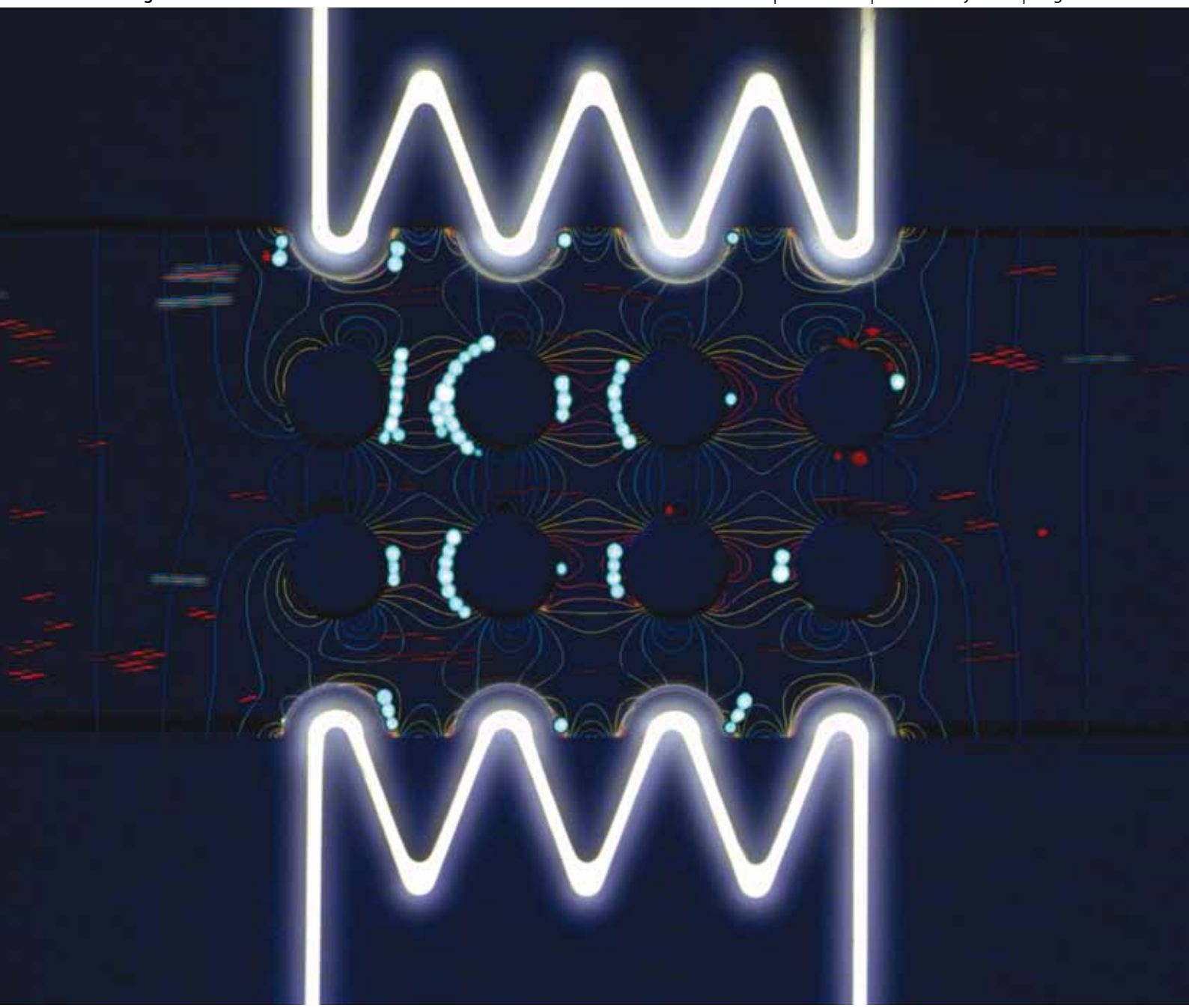

ISSN 1473-0197

RSC Publishing

Celebrating 10 Years of publishing

1473-0197(2010)10:4;1-D

Selective isolation of live/dead cells using contactless dielectrophoresis (cDEP)†

Hadi Shafiee,[ad] Michael B. Sano,‡[abd] Erin A. Henslee,‡[bd] John L. Caldwell[cd] and Rafael V. Davalos*[abd]

Received 2nd October 2009, Accepted 14th December 2009
First published as an Advance Article on the web 19th January 2010
DOI: 10.1039/b920590j

Contactless dielectrophoresis (cDEP) is a recently developed method of cell manipulation in which the electrodes are physically isolated from the sample. Here we present two microfluidic devices capable of selectively isolating live human leukemia cells from dead cells utilizing their electrical signatures. The effect of different voltages and frequencies on the gradient of the electric field and device performance was investigated numerically and validated experimentally. With these prototype devices we were able to achieve greater than 95% removal efficiency at 0.2–0.5 mm s^{-1} with 100% selectivity between live and dead cells. In conjunction with enrichment, cDEP could be integrated with other technologies to yield fully automated lab-on-a-chip systems capable of sensing, sorting, and identifying rare cells.

Introduction

Isolation and enrichment of cells/microparticles from a biological sample is one of the first crucial processes in many biomedical and homeland security applications.[1] Water quality analysis to detect viable pathogenic bacterium[2–6] and the isolation of rare circulating tumor cells (CTCs) for early cancer detection[7–19] are important examples of the applications of this process.

Dielectrophoresis (DEP) is the motion of a particle in a suspending medium due to the presence of a non-uniform electric field.[20,21] DEP utilizes the electrical properties of the cell/particle for separation and identification.[21,22] The physical and electrical properties of the cell, the conductivity and permittivity of the media, as well as the gradient of the electric field and its applied frequency are substantial parameters determining a cell's DEP response.

One unique advantage of DEP over existing methods for cell separation is that the DEP force is strongly dependent on cell viability. The cell membrane, which is normally impermeable and highly insulating, typically becomes permeable after cell death.[23] This results in the release of ions from the cytoplasm through the structural defects in the dead cell membrane and the cell conductivity will increase dramatically.[24] This alteration in electrical properties after cell death make DEP live/dead cell separation and isolation possible.

The utilization of DEP to manipulate live and dead cells has previously been demonstrated through several approaches. To start, Suehiro *et al.* were able to utilize dielectrophoretic impedance measurements to selectively detect viable bacteria.[25] Conventional interdigitated electrode DEP microdevices have also been used to separate live and heat-treated Listeria cells.[26] Huang *et al.* investigated the difference in the AC electrodynamics of viable and non-viable yeast cells through DEP and electrorotation experiments[27] and a DEP-based microfluidic device for the selective retention of viable cells in culture media with high conductivity was proposed by Docoslis *et al.*[28]

Insulator-based dielectrophoresis (iDEP) has also been employed to concentrate and separate live and dead bacteria for water analysis.[2] In this method, electrodes inserted into a microfluidic channel create an electric field which is distorted by the presence of insulating structures. The devices can be manufactured using simple fabrication techniques and can be mass-produced inexpensively through injection molding or hot embossing.[29,30] iDEP provides an excellent solution to the complex fabrication required by traditional DEP devices, however, it is difficult to utilize for biological fluids which are highly conductive. The challenges that arise include joule heating and bubble formation.[31] In order to mitigate these effects, the electrodes are often placed in large reservoirs at the channel inlet and outlet. Without an additional channel for the concentrated sample,[30] this could re-dilute the sample after it has passed through a concentrated region.

The authors have recently developed a robust, simple, and inexpensive technique to perform DEP, termed "contactless dielectrophoresis" (cDEP). This technique provides the non-uniform electric fields in microfluidic channels required for DEP cell manipulation without direct contact between the electrodes and the sample.[32] In this method, an electric field is created in the sample microchannel using electrodes inserted into two conductive microchambers, which are separated from the sample channel by thin insulating barriers. These insulating barriers exhibit a capacitive behavior and therefore an electric field can be produced in the main channel by applying an AC field across the barriers.[32]

The absence of contact between the electrodes and the sample fluid prevents problems associated with more conventional approaches to DEP and iDEP including contamination,

[a]*Engineering Science and Mechanics Department, Virginia Tech, Blacksburg, VA, 24061. E-mail: shafiee@vt.edu*
[b]*School of Biomedical Engineering & Sciences, Virginia Tech – Wake Forest University, Blacksburg, VA, 24061*
[c]*Bradley Department of Electrical and Computer Engineering, Virginia Tech, Blacksburg, VA, 24061*
[d]*Bioelectromechanical Systems Laboratory, Institute for Critical Technology and Applied Science (ICTAS), Virginia Tech, VA, 24061. E-mail: davalos@vt.edu; Tel: 1-540-231-1979*

† Electronic supplementary information (ESI) available: Cell sorting with cDEP (supplemental videos 1 and 2). See DOI: 10.1039/b920590j
‡ Both authors contributed equally to the work.

 This journal is © The Royal Society of Chemistry 2010

electrochemical effects, bubble formation, and the detrimental effects of joule heating.[33] Similar to iDEP, cDEP lends itself to a much simpler fabrication procedure. Devices are typically molded from a reusable silicon master stamp that has been fabricated from a single-mask lithographic process. Once the master stamp has been fabricated, cDEP devices can be produced from the stamp outside of the cleanroom environment, allowing for rapid, mass fabrication of cDEP microfluidic devices.

In this study, the ability of cDEP to selectively isolate and enrich a cell population was investigated. This was demonstrated through the separation of viable cells from a heterogeneous population also containing dead cells. Two cDEP microfluidic devices were designed and fabricated out of polydimethylsiloxane (PDMS) and glass using standard photolithography. The DEP response of the cells was investigated under various electrical experimental conditions in the range of our power supply limitations. Human leukemia THP-1 viable cells were successfully isolated from dead (heat treated) cells without lysing.

The separation of viable and non-viable cells is a critical starting point for this new technology to move towards more advanced applications. Optimization of these devices would allow for selective separation of cells from biological fluids for purposes such as: the diagnosis of early stages of diseases, drug screening, sample preparation for downstream analysis, enrichment of tumor cells to evaluate tumor lineage *via* PCR, as well as treatment planning.[34–39] By using viable/non-viable separation as a model for these applications, a new generation of cDEP devices can be tailored around the results reported in this study.

Theory

The 3D schematic of the experimental set up for device 1 is shown in Fig. 1. The dominant forces acting on the cell/particle in the microfluidic devices are shown in Fig. 2a and 3a. For particles larger than 1 μm, Brownian motion is negligible compared to the DEP force.[1] The DEP force acting on a spherical particle can be described by the following:[1,20,40]

$$F_{DEP} = 2\pi\epsilon_m r^3 \mathrm{Re}[f_{CM}]\nabla|E|^2 \quad (1)$$

where ϵ_m is the permittivity of the suspending medium, r is the radius of the particle, $\nabla|E|^2$ defines the local electric field gradient, Re[] represents the real part, and f_{CM} is the Clausius–Mossotti factor given by:

$$f_{CM} = \frac{\bar{\varepsilon}_p - \bar{\varepsilon}_m}{\bar{\varepsilon}_p + 2\bar{\varepsilon}_m} \quad (2)$$

where $\bar{\varepsilon}_p$ and $\bar{\varepsilon}_m$ are the particle and the medium complex permittivity respectively. The complex permittivity is defined as follows:

$$\bar{\varepsilon} = \varepsilon - j\frac{\sigma}{\omega} \quad (3)$$

where ϵ is the permittivity, σ is the conductivity, $j^2 = -1$, and ω is the angular frequency. Using the complex permittivity given in eqn (3) of the particle and medium, the real part of Clausius–Mossotti factor is calculated as follows:[41]

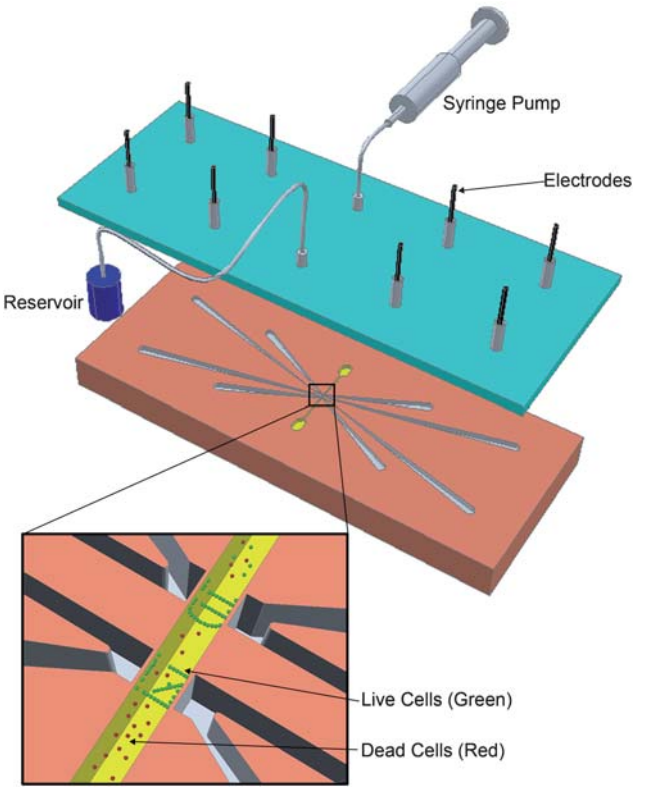

Fig. 1 3D schematic of the experimental set up.

$$\mathrm{Re}[f_{CM}] = \frac{(\sigma_p - \sigma_m)}{(1+\omega^2\tau^2)(\sigma_p + 2\sigma_m)} + \frac{\omega^2\tau^2(\varepsilon_p - \varepsilon_m)}{(1+\omega^2\tau^2)(\varepsilon_p + 2\varepsilon_m)} \quad (4)$$

where τ is the Maxwell–Wagner constant.

For cells, the complex permittivity can be estimated using a single shell model, which is given by:

$$\bar{\varepsilon}_p = \bar{\varepsilon}_{mem}\frac{\gamma^3 + 2\left(\frac{\bar{\varepsilon}_i - \bar{\varepsilon}_{mem}}{\bar{\varepsilon}_i + 2\bar{\varepsilon}_{mem}}\right)}{\gamma^3 - \left(\frac{\bar{\varepsilon}_i - \bar{\varepsilon}_{mem}}{\bar{\varepsilon}_i + 2\bar{\varepsilon}_{mem}}\right)} \quad (5)$$

where $\gamma = \frac{r}{r-d}$, r is the particle radius, d is the cell membrane thickness, $\bar{\varepsilon}_i$ and $\bar{\varepsilon}_{mem}$ are the complex permittivites of the cytoplasm and the membrane, respectively.[1,41]

The parabolic velocity profile in the microchannel, shown in Fig. 2a and 3a, is due to the low Reynolds number pressure driven flow across the main channel. Assuming the cell as a spherical particle, the hydrodynamic drag force due to cell translation is given by:

$$f_{Drag} = 6\eta r\pi(u_p - u_f) \quad (6)$$

where r is the particle radius, η is the medium viscosity, u_p is the velocity of the particle, and u_f is the medium velocity. Others have shown that for microparticles moving in viscous environments, the inertial forces are negligible.[42] The characteristic time for a spherical particle suspended in fluid is reported to be

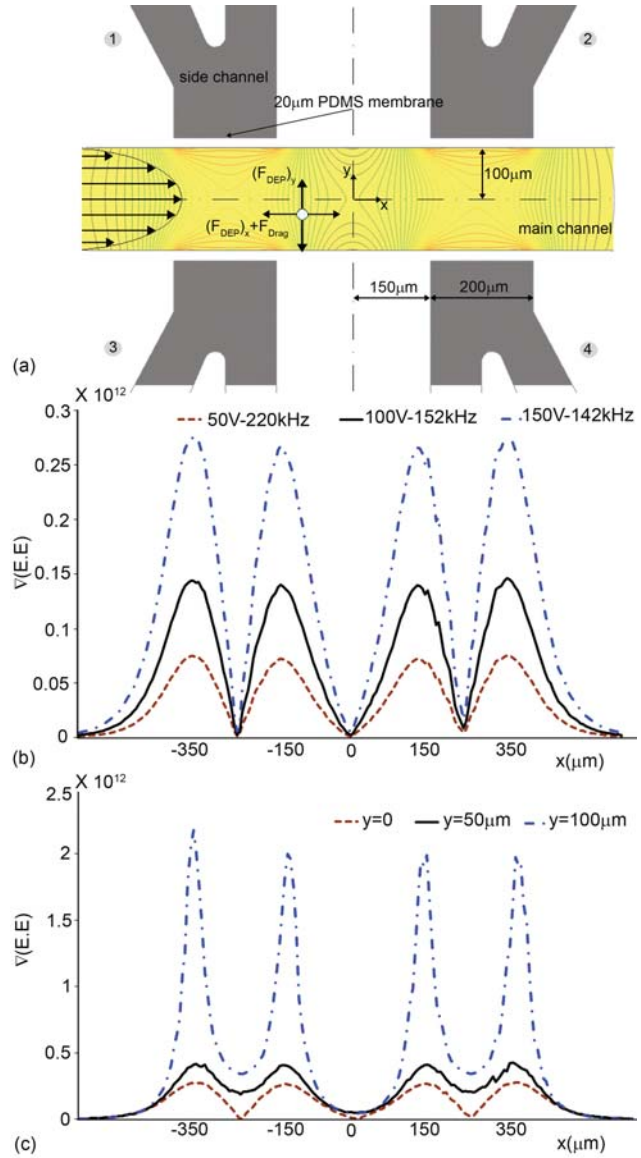

Fig. 2 (a) 2D top view schematic of device 1 showing the dominant forces acting on the particle. The contours represent the electric fields modelled in Comsol multiphysics. (b) Line plot of the gradient of the electric field squared (kg^2 m C^{-2} S^{-4}) for three different electrical boundary conditions with efficient numerical cell trapping ($V_1 = V_2 = 50$ V_{rms} at 220 kHz, 100 V_{rms} at 152 kHz, and 150 V_{rms} at 142 kHz and $V_3 = V_4 =$ Ground). (c) Line plot of the gradient of the electric field squared (kg^2 m C^{-2} S^{-4}) along the lines parallel to the center line of the main channel and at different distances from the channel wall for $V_1 = V_2 =$ 150 V_{rms} at 142 kHz boundary condition ($y = 0$, 50, and 100 μm).

$\frac{2\rho r^2}{9\eta}$, where ρ is the density of the medium, r is radius of the particle, and η is the viscosity of the medium.

For THP-1 cells with a 15.4 ± 2 μm diameter[32] this characteristic time would be 12 μs, which is orders of magnitude smaller than the time scale of the external forces and our experimental observations. The velocity of the particle is determined by a balance between the DEP force and Stoke's drag force. The relationship is given by:

$$u_p = u_f - \mu_{DEP}\nabla(E\cdot E) \quad (7)$$

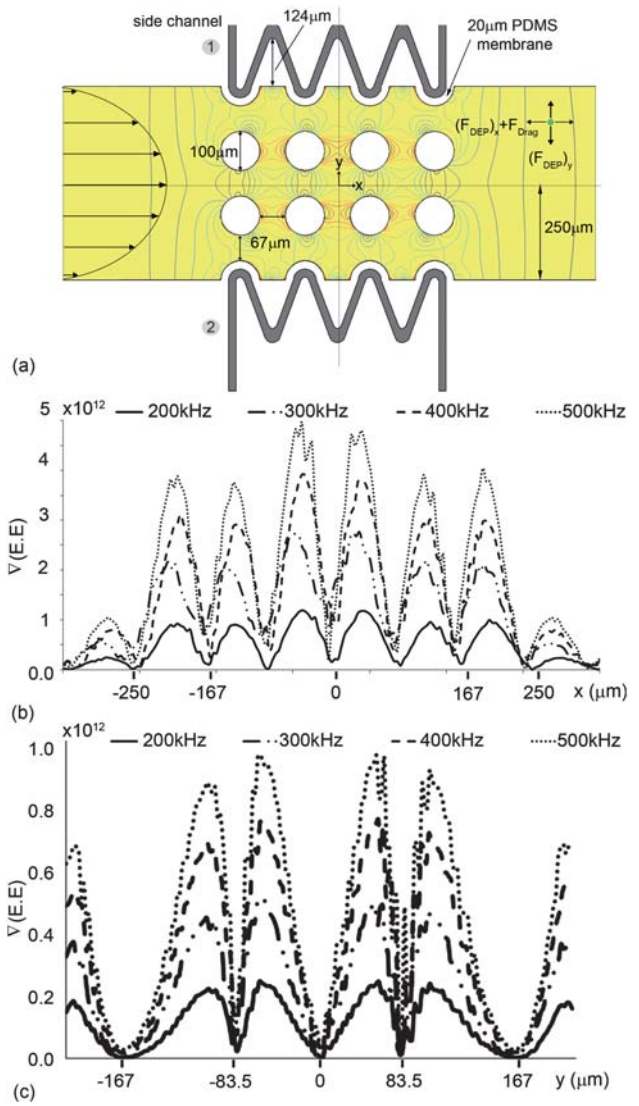

Fig. 3 (a) 2D top view schematic of device 2, showing the dominant forces acting on the particle. The contours represent the electric fields modelled in Comsol multiphysics. (b) Line plot of the gradient of the electric field squared (kg^2 m C^{-2} S^{-4}) for four different electrical boundary conditions with efficient numerical cell trapping (V_1 = 30 V_{rms} at 200 kHz, 300 kHz, 400 kHz, and 500 kHz, V_2 = Ground) along the x axis ($y = 0$). (c) Line plot of the gradient of the electric field squared (kg^2 m C^{-2} S^{-4}) for four different electrical boundary conditions with efficient numerical cell trapping ($V_1 = 30$ V_{rms} at 200 kHz, 300 kHz, 400 kHz, and 500 kHz, and V_2 = Ground) along the y axis ($x = 0$).

where μ_{DEP} is the dielectrophoretic mobility of the particle and is defined as:

$$\mu_{DEP} = \frac{\varepsilon_m r^2}{3\eta}\mathrm{Re}[f_{CM}] \quad (8)$$

Methods

Fabrication

A silicon master stamp was fabricated on a <100> silicon substrate following our previously described process.[32] Deep

This journal is © The Royal Society of Chemistry 2010

reactive ion etching (DRIE) was used to etch the silicon master stamp to a depth of 50 μm. Silicon oxide was grown on the silicon master using thermal oxidation for four hours at 1000 °C and removed with HF solvent to reduce surface scalloping. Liquid phase polydimethylsiloxane (PDMS) was made by mixing the PDMS monomers and the curing agent in a 10 : 1 ratio (Sylgard 184, Dow Corning, USA). The degassed PDMS liquid was poured onto the silicon master, cured for 45 min at 100 °C, and then removed from the mold. Fluidic connections to the channels were punched using hole punchers (Harris Uni-Core, Ted Pella Inc., Redding, CA); 1.5 mm for the side channels and 2.0 mm for the main channel inlet and outlet. Microscope glass slides (75 mm × 75 mm × 1.2 mm, Alexis Scientific) were cleaned with soap and water, rinsed with distilled water, ethanol, isopropyl alcohol, and then dried with compressed air. The PDMS mold was bonded to clean glass after treating with air plasma for 2 min. Schematics of the devices with dimensions are shown in Fig. 2a and 3a.

Cell preparation

The live samples of THP-1 human leukemia monocytes were washed twice and resuspended in a buffer used for DEP experiments (8.5% sucrose [wt/vol], 0.3% glucose [wt/vol], and 0.725% RPMI [wt/vol] [43]) to 10^6 cells mL^{-1}. The cell samples to be killed were first pipetted into a conical tube and heated in a 60 °C water bath for 12 min; an adequate time determined to kill the majority of the cells in the sample.

To enable simultaneous observation under fluorescent microscope, cells were stained using a LIVE/DEAD® Viability/Cytotoxicity Kit for mammalian cells (Molecular Probes Inc.). Calcein AM, which is enzymatically converted to green fluorescent calcein, was added to the live cell sample at 2 μL per mL of cell suspension. Ethidium homodimer-1 (EthD-1) was added to the dead cell sample at 6 μL per mL of cell suspension. This can only pass through damaged cell membranes and upon nucleic acid-binding produces a red fluorescence.

The two samples were then vortexed for 5 min, washed once and resuspended in DEP buffer. The live and dead suspensions were then mixed together in one conical tube with a final concentration of 10^6 cells mL^{-1} and final conductivity of 110–115 μS cm^{-1} measured with a SevenGo Pro conductivity meter (Mettler-Toledo, Inc., Columbus, OH). Live and dead cells were indistinguishable under bright field evaluation.

Experimental set-up

The microfluidic devices were placed in a vacuum jar for 30 min prior to experiments to reduce problems associated with priming. Pipette tips were used to fill the side channels with phosphate buffered saline (PBS) and acted as reservoirs. Aluminium electrodes were placed in the side channel reservoirs. The electrodes inserted in side channels 1 and 2 of device 1 (Fig. 2a) were used for excitation while the electrodes inserted in side channels 3 and 4 were grounded. The electrodes inserted in side channel 1 of device 2 (Fig. 3a) were used for excitation while the electrodes inserted in side channel 2 were grounded. Thin walled Teflon tubing (Cole-Parmer Instrument Co., Vernon Hills, IL) was inserted into the inlet and outlet of the main channel. A 1 mL syringe containing the cell suspension was fastened to a microsyringe pump (Cole Parmer, Vernon Hills, IL) and connected to the inlet tubing. Once the main channel was primed with the cell suspension, the syringe pump was set to 0.02 mL h^{-1}; equivalent to a velocity of 556 μm s^{-1} for device 1 and 222 μm s^{-1} for device 2. This flow rate was maintained for 5 min prior to experiments.

An inverted light microscope (Leica DMI 6000B, Leica Microsystems, Bannockburn, IL) equipped with a color camera (Leica DFC420, Leica Microsystems, Bannockburn, IL) was used to monitor the cells flowing through the main channel. Once the flow rate of 0.02 mL h^{-1} was maintained for 5 min an AC electric field was applied to the electrodes.

Device 1. Experiments were conducted at 50 V_{rms}, 75 V_{rms}, 100 V_{rms}, 125 V_{rms} and 150 V_{rms}. Trapping boundary conditions for this device were determined through visual inspection of the cells passing through the main channel. At each voltage, the frequency was recorded for 80% trapping and the onset of cell lysis. Significant lysis was considered to be when at least 10% of the cell population became lysed. The electric field was maintained for 30 s during each experiment. Eight trials were conducted at each voltage and the corresponding frequencies were recorded where 80% trapping was observed.

Device 2. The trapping efficiency for this device was determined for voltages of 20 V_{rms}, 30 V_{rms}, 40 V_{rms}, 50 V_{rms} and frequencies of 200 kHz, 300 kHz, 400 kHz, 500 kHz at a constant flow rate of 0.02 mL h^{-1}. Experimental parameters were tested at random to mitigate any variation in cell concentration, flow rate, device functionality and other experimental variables. Additionally, trapping efficiency was calculated at 0.02 mL h^{-1}, 0.04 mL h^{-1}, 0.06 mL h^{-1}, and 0.08 mL h^{-1}, with electrical parameters held constant at 500 kHz and 30 V_{rms}. Electrical parameters were selected randomly for each experiment for a total of five trials at each combination. The electric field was maintained for 30 s during each experiment. During the 30 s interval, all cells entering the trapping region of the device (the region containing pillars in the main channel) were counted, representing the total number of cells.

Electrical equipment

AC electric fields were applied to the microfluidic devices using a combination of waveform generation and amplification equipment. Waveform generation was performed by a function generator (GFG-3015, GW Instek, Taipei, Taiwan) whose output was then fed to a wideband power amplifier (AL-50HF-A, Amp-Line Corp., Oakland Gardens, NY). The wideband power amplifier performed the initial voltage amplification of the signal and provided the necessary output current to drive a custom-wound high-voltage transformer (Amp-Line Corp., Oakland Gardens, NY). This transformer was placed inside a grounded cage and attached to the devices using high-voltage wiring. Frequency and voltage measurements were accomplished using an oscilloscope (TDS-1002B, Tektronics Inc. Beaverton, OR) connected to a 100 : 1 voltage divider at the output of the transformer.

Numerical modeling

The electric field distribution and its gradient $\nabla E = \nabla(\nabla\phi)$ were modeled numerically in Comsol multi-physics 3.5 using the AC/DC module (Comsol Inc., Burlington, MA, USA). This is done by solving for the potential distribution, ϕ, using the governing equation, $\nabla\cdot(\sigma^*\nabla\phi) = 0$, where σ^* is the complex conductivity ($\sigma^* = \sigma + j\omega\epsilon$) of the sub-domains in the microfluidic devices. The boundary conditions used are prescribed uniform potentials at the inlet or outlet of the side channels.

The values for the electrical conductivity and permittivity of the PDMS, PBS, and DEP buffer that were used in this numerical modeling are given in Table 1. PBS and DEP buffer electrical properties are used for the side and main microfluidic channels, respectively. The induced DEP effect inside the main channel was investigated for a range of frequencies and voltages. The gradient of the electric field along the center line ($y = 0$) of the main channel as well as $y = 50$ μm and $y = 100$ μm was investigated numerically.

Results and discussion

Device 1

The geometry of device 1 allowed for the rapid simulation of DEP effects within the sample microchannel which could then be verified through an efficient fabrication and experimentation procedure. The gradient of the electric field along the center line of the main channel of device 1 was numerically modeled and the results are plotted in Fig. 2b. Fig. 2b also shows that the maximum gradient of the electric field occurs at the terminations of the side channels. The dependence of the gradient of the electric field in the main channel on distance from the channel wall is shown in Fig. 2c. These numerical results indicate that the gradient of the electric field and thus the DEP effect is strongly related to the channel geometry.

Conclusions drawn from the numerical modeling of device 1 were verified through direct experimentation. Live cell concentration and trapping was observed for the electrical boundary conditions that were previously simulated ($V_1 = V_2 = 50$ V_{rms} at 220 kHz, 100 V_{rms} at 152 kHz, and 150 V_{rms} at 142 kHz and $V_3 = V_4$ = Ground). A large DEP response was achieved with an applied voltage of 150 V_{rms} at 142 kHz, mirroring the numerical modeling shown in Fig. 2b. The majority of cell trapping within the device occurred at the edges of the electrodes as predicted by numerical results found in Fig. 2b.

When 80% trapping was observed, cells closest to the channel wall were trapped while those closer to the center of the channel were not; a result predicted by the numerical modeling presented in Fig. 2c. These simulations further indicated that at low frequencies (≤100 kHz) the gradient of the electric field inside the main channel would not be sufficient for DEP cell manipulation and this was confirmed in our experiments. The minimum frequency necessary to achieve an 80% trapping efficiency is given in Fig. 4a as a function of applied voltage. Cell lysing was observed for 75 V_{rms}, 100 V_{rms}, 125 V_{rms}, and 150 V_{rms} at 296 kHz, 243 kHz, 197 kHz, and 173 kHz, respectively. No lysing was observed at 50 V_{rms} within the frequency limits of the power supply. The concentration of live THP-1 cells using a 150 kHz voltage signal at 100 V_{rms} in device 1 is shown in Fig. 5 and a representative video is given in the ESI† (supplemental video 1).

Table 1 Electrical properties of the materials and fluids

	Electrical Properties	
Materials	Electrical Conductivity/S m^{-1}	Relative Electrical Permittivity
PDMS	0.83×10^{-12}	2.65
PBS	1.4	80
DEP buffer	0.01	80

Device 2

Since numerical modeling proved valid for device 1, it was also used to predict the performance of device 2. The gradient of the electric field along the x-axis ($y = 0$) of the main channel of device 2 is plotted in Fig. 3b. Again, for these electrical boundary conditions ($V_1 = 30$ V_{rms} at 200 kHz, 300 kHz, 400 kHz, and 500 kHz and V_2 = Ground) cell trapping was observed. Local maximums in the gradient of the electric field occurred in line with the edges of the insulating pillars while the minimum gradient was experienced as cells passed through the region between two pillars. The highest electric field gradient was observed to occur at the two insulating pillars which had edges in the center of the device. The electric field gradients in the center of device 2 along the y-axis ($x = 0$) are shown in Fig. 3c and the highest gradient was observed in line with the edges of the insulating pillars. It should be noted that the maximum gradient is observed at $y = \pm 83.5$ μm and cells traveling through the exact center of the device (along the x-axis) experience a lower DEP force than those just off-center. The electric field gradient within the channel increased with applied signal frequency from 200 kHz to 500 kHz. This increase in gradient is not linear and these parameters represent the limitations of our current electrical setup.

Theoretically, device 2 has a maximum gradient of electric field within the channel occurring between 600 kHz and 700 kHz as seen in Fig. 4d. Above this frequency, leakages in the system begin to dominate the response and the electric field within the channel drops off.

Live THP-1 cells were observed to experience a positive DEP force at the reported frequencies and the DEP force applied on dead cells appeared to be negligible. In device 2, the majority of cell trapping was observed in the region between the first two columns of insulating barriers at 0.02 mL h^{-1}. However, the distribution of trapped cells became more uniform at higher flow rates. At 0.02 mL h^{-1}, we observed trapping efficiencies greater than 90% at all tested frequencies (200 kHz, 300 kHz, 400 kHz, and 500 kHz). However, lysing was seen at all frequencies when a voltage of 50 V_{rms} was applied. At the highest two frequencies, lysing was seen at 40 V_{rms} and over 10% of the cells lysed at 50 V_{rms} (Fig. 4c). Aside from lysing, the maximum voltage we are able to apply to these devices is determined by the electrical breakdown voltage of the PDMS composing the barriers. Our results suggest that the performance of our cDEP devices is comparable to and may be able to exceed what is currently attainable and has been reported with DEP or iDEP.[14,28,44,45]

This journal is © The Royal Society of Chemistry 2010

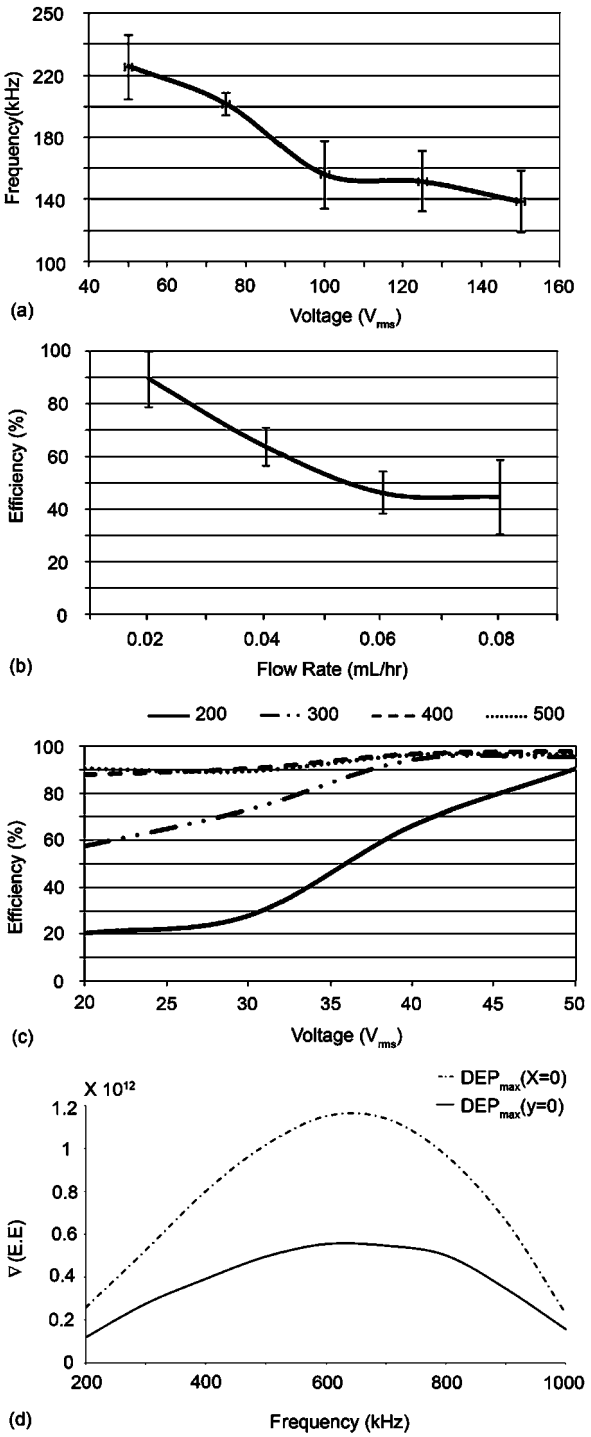

Fig. 4 (a) Voltage–frequency pairs to achieve 80% trapping efficiency for device 1. (b) Trapping efficiency of device 2 at 500 kHz and 30 V_{rms} for flow rates of 0.02, 0.04, 0.06, and 0.08 mL h^{-1}. (c) Trapping efficiency at 0.02 mL h^{-1} of device 2 at 200, 300, 400, and 500 kHz as voltages increase from 20 V_{rms} to 50 V_{rms}. (d) Maximum gradient of the electric field along the x ($y = 0$) and y ($x = 0$) axis of device 2 for frequencies between 200 kHz and 1000 kHz.

In device 2, a maximum of 50 V_{rms} at 500 kHz signal was applied to the inlets of the electrode channels. Because the sample channel is non-uniform, it was found through our numerical results that the actual electric field experienced by cells within the channel was between 20 V cm^{-1} and 200 V cm^{-1}. However, there are minute regions at the sharp corners inside the main channel with a high electric field intensity (~350 V cm^{-1}) that induces electroporation (IRE),[46,47] which is what we have observed during the experiments. This was caused by the dramatic change in the thickness of the PDMS barrier in those locations. It was in these small regions which cell lysing was most commonly seen.

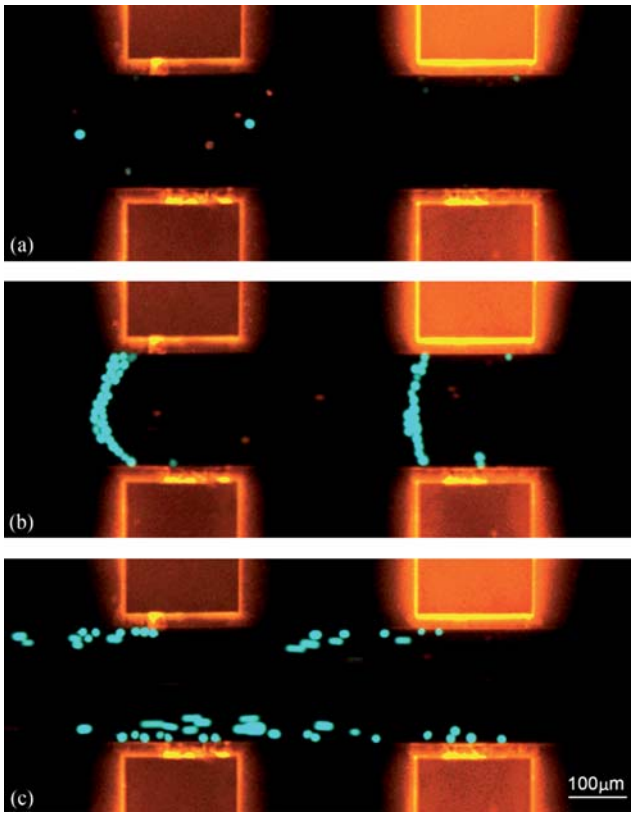

Fig. 5 Experimental results for device 1: (a) Dead (red) and live (blue/green) THP-1 cells are moving from right to left due to pressure driven flow without applying an electric field. (b) 30 s after applying the electric field ($V_1 = V_2 = 100$ V_{rms} at 152 kHz and $V_3 = V_4 =$ Ground). The live (blue/green) cells were trapped due to positive DEP, but the dead (red) cells pass by the trapping area. (c) Releasing the trapped live cells by turning off the power supply. Side channels are fluorescent due to Rhodamine B dye suspended in PBS.

Trapping efficiency experiments for higher flow rates were conducted at 500 kHz and 30 V_{rms} because these parameters yielded a high trapping efficiency of 89.6% at 0.02 mL h^{-1}. The trapping efficiency was reduced by an increase in flow rate and reached a minimum of 44.8% (± 14.2) at 0.8 mL h^{-1} (Fig. 4b). Flow rates greater than 0.1 mL h^{-1} were not reported due to limitations of our recording software that resulted in the inability to accurately count the number of cells entering and exiting the trapping region of the device.

Due to the capacitance effect of the PDMS barriers in cDEP devices, the corresponding gradient of the electric field for voltage–frequency pairs are different for each design. These devices were designed to provide a sufficient gradient of the electric field for DEP cell manipulation within the limitations of our power supply and the PDMS breakdown voltage. The high

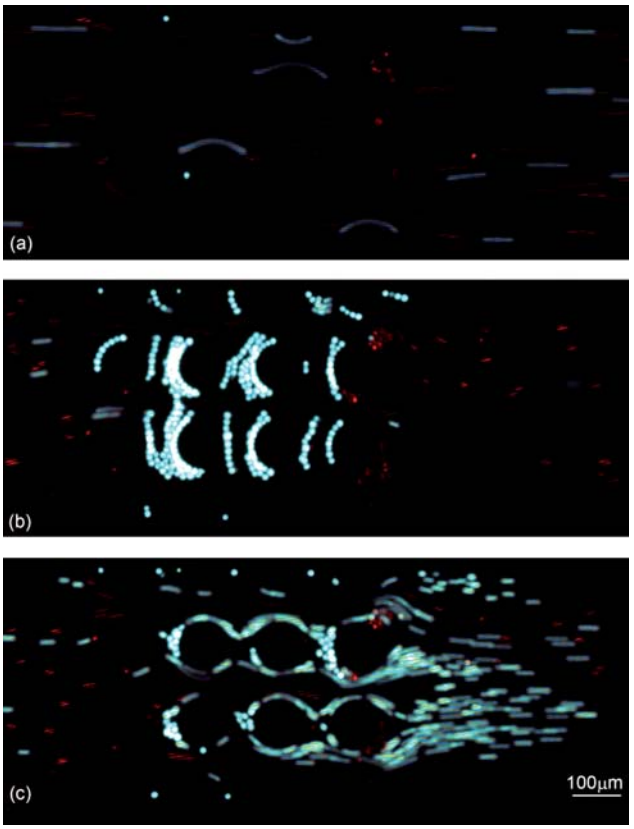

Fig. 6 Experimental results for device 2: (a) dead (red) and live (blue/green) THP-1 cells are moving from left to right due to pressure driven flow. (b) 30 s after applying the electric field ($V_1 = 40$ V_{rms} at 500 kHz and V_2 = Ground) live cells were trapped due to positive DEP but dead cells pass by. (c) Releasing the trapped live cells by turning off the power supply.

trapping efficiency makes device 2 an optimal design for selective entrapment and enrichment of cell samples. This process is depicted in Fig. 6; initially live cells (green) and dead cells (red) passed through the trapping region due to pressure driven flow (Fig. 6a). Live cells were selectively concentrated in the trapping region under the application of a 500 kHz, 40 V_{rms} signal (Fig. 6b). Under these parameters, the DEP force on the dead cells was not sufficient to influence their motion and they passed through the trapping region. The enriched sample of live cells can be controllably released for later analysis once the electric field is turned off (Fig. 6c). A representative video is given in the ESI† (supplemental video 2).

Conclusion

This work has demonstrated the ability of cDEP to selectively concentrate specific cells from diverse populations through the separation of viable cells from a sample containing both viable and non-viable human leukemia cells. Repeatability, high efficiency, sterility, and an inexpensive fabrication process are benefits inherent to cDEP over more conventional methods of cell separation. This method is also unique in that direct evaluation is possible with little or no sample preparation. The resulting time and material savings are invaluable in homeland security and biomedical applications. Given cDEP's numerous advantages, the technique has tremendous potential for sample isolation and enrichment for drug screening, disease detection and treatment, and other lab-on-a-chip applications.

Acknowledgements

This work was supported in part by the Institute for Critical Technology and Applied Science (ICTAS). We acknowledge Phillip A. Zellner and Joseph D. Mock for their technical support.

References

1 H. Morgan and N. G. Green, *AC Electrokinetics: Colloids and Nanoparticles*, Research Studies Press LTD, Hertfordshire, England, 2003.
2 B. H. Lapizco-Encinas, B. A. Simmons, E. B. Cummings and Y. Fintschenko, *Anal. Chem.*, 2004, **76**, 1571–1579.
3 D. Armstrong, J. Schneiderheinze, J. Kullman and L. He, *FEMS Microbiol. Lett.*, 2001, **194**, 33–37.
4 D. Armstrong, G. Schulte, J. Schneiderheinze and D. Westenberg, *Anal. Chem.*, 1999, **71**, 5465–5469.
5 M. Girod and D. W. Armstrong, *Electrophoresis*, 2002, **23**, 2048–2056.
6 C. R. Cabrera and P. Yager, *Electrophoresis*, 2001, **22**, 355–362.
7 F. F. Becker, X.-B. Wang, Y. Huang, R. Pethig, J. Vykoukal and P. R. C. Gascoyne, *J. Phys. D: Appl. Phys.*, 1994, **27**, 2659–2662.
8 P. R. C. Gascoyne, X.-B. Wang, Y. Huang and F. F. Becker, *IEEE Trans. Ind. Appl.*, 1997, **33**, 670–678.
9 Y. Huang, S. Joo, M. Duhon, M. Heller, B. Wallace and X. Xu, *Anal. Chem.*, 2002, **74**, 3362–3371.
10 J. Cheng, E. L. Sheldon, L. Wu, M. J. Heller and J. P. O'Connell, *Anal. Chem.*, 1998, **70**, 2321–2326.
11 L. Altomare, M. Borgatti, G. Medoro, N. Manaresi, M. Tartagni, R. Guerrieri and R. Gambari, *Biotechnol. Bioeng.*, 2003, **82**, 474–479.
12 G. H. Markx, M. S. Talary and R. Pethig, *J. Biotechnol.*, 1994, **32**, 29–37.
13 C. M. Das, F. Becker, S. Vernon, J. Noshari, C. Joyce and P. R. Gascoyne, *Anal. Chem.*, 2005, **77**, 2708–2719.
14 P. R. Gascoyne, J. Noshari, T. J. Anderson and F. F. Becker, *Electrophoresis*, 2009, **30**, 1388–1398.
15 S. Apostolaki, M. Perraki, A. Pallis, V. Bozionelou, S. Agelaki, P. Kanellou, A. Kotsakis, E. Politaki, K. Kalbakis, A. Kalykaki, L. Vamvakas, V. Georgoulias and D. Mavroudis, *Ann. Oncol.*, 2007, **18**, 851–858.
16 M. Cristofanilli, *Cancer*, 2005, **103**, 877–880.
17 K. Fizazi, L. Morat, L. Chauveinc, D. Prapotnich, R. De Crevoisier, B. Escudier, X. Cathelineau, F. Rozet, G. Vallancien, L. Sabatier and J. C. Soria, *Ann. Oncol.*, 2007, **18**, 518–521.
18 D. F. Hayes, M. Cristofanilli, G. T. Budd, M. J. Ellis, A. Stopeck, M. C. Miller, J. Matera, W. J. Allard, G. V. Doyle and L. W. Terstappen, *Clin. Cancer Res.*, 2006, **12**, 4218–4224.
19 M. Naoe, Y. Ogawa, J. Morita, K. Omori, K. Takeshita, T. Shichijyo, T. Okumura, A. Igarashi, A. Yanaihara, S. Iwamoto, T. Fukagai, A. Miyazaki and H. Yoshida, *Cancer*, 2007, **109**, 1439–1445.
20 H. Pohl, *J. Appl. Phys.*, 1951, **22**, 869–871.
21 H. A. Pohl, *J. Appl. Phys.*, 1958, **29**, 1182–1188.
22 H. Pohl, *Dielectrophoresis*, Cambridge University Press, Cambridge, 1978.
23 R. V. Davalos and B. Rubinsky, *J. Biomech. Eng.*, 2004, **126**, 305–309.
24 C. P. Jen and T. W. Chen, *Biomed. Microdevices*, 2009, **11**, 597–607.
25 J. Suehiro, R. Hamada, D. Noutomi, M. Shutou and M. Hara, *J. Electrost.*, 2003, **57**, 157–168.
26 H. Li and R. Bashir, *Sens. Actuators, B*, 2002, **86**, 215–221.
27 Y. Huang, R. Holzel, R. Pethig and X. B. Wang, *Phys. Med. Biol.*, 1992, **37**, 1499–1517.
28 A. Docoslis, N. Kalogerakis, L. A. Behie and K. V. Kaler, *Biotechnol. Bioeng.*, 1997, **54**, 239–250.
29 B. A. Simmons, G. J. McGraw, R. V. Davalos, G. J. Fiechtner, Y. Fintschenko and E. B. Cummings, *MRS Bulletin*, 2006, **31**, 120–124.

 This journal is © The Royal Society of Chemistry 2010

30 P. Sabounchi, A. M. Morales, P. Ponce, L. P. Lee, B. A. Simmons and R. V. Davalos, *Biomed. Microdevices*, 2008, **10**, 661–670.
31 Y. Kang, D. Li, S. A. Kalams and J. E. Eid, *Biomed. Microdevices*, 2008, **10**, 243–249.
32 H. Shafiee, J. L. Caldwell, M. B. Sano and R. V. Davalos, *Biomed. Microdevices*, 2009, **11**, 997–1006.
33 F. S. Steffen Hardt, *Microfluidic Technologies for Miniaturized Analysis Systems*, Springer, New York, NY, 2007.
34 M. Borgatti, R. Rizzo, I. Mancini, E. Fabbri, O. Baricordi and R. Gambari, *Minerva Biotechnol.*, 2007, **19**, 71–74.
35 F. Del Bene, M. Germani, G. De Nicolao, P. Magni, C. E. Re, D. Ballinari and M. Rocchetti, *Cancer Chemother. Pharmacol.*, 2009, **63**, 827–836.
36 T. G. Ntouroupi, S. Q. Ashraf, S. B. McGregor, B. W. Turney, A. Seppo, Y. Kim, X. Wang, M. W. Kilpatrick, P. Tsipouras, T. Tafas and W. F. Bodmer, *Br. J. Cancer*, 2008, **99**, 789–795.
37 S. V. Sarantseva and A. L. Schwarzman, *Russ. J. Genet.*, 2009, **45**, 761–770.
38 D. A. Tatosian and M. L. Shuler, *Biotechnol. Bioeng.*, 2009, **103**, 187–198.
39 J. F. Leary, L. N. Reece, P. Szaniszlo, T. Prow and N. Wang, in *Conference on Clinical Diagnostic Systems*, ed. G. E. Cohn, Spie-Int Soc Optical Engineering, San Jose, Ca, 2001, pp. 16–27.
40 T. B. Jones, *Electromechanics of Particles*, Cambridge University Press, USA, 1995.
41 H. Morgan, T. Sun and D. Holmes, *J. Phys. D: Appl. Phys.*, 2007, **40**, 61–70.
42 H. Bruus, *Theoretical Microfluidics*, Oxford University Press Inc., NY, 2008.
43 L. A. Flanagan, J. Lu, L. Wang, S. A. Marchenko, N. L. Jeon, A. P. Lee and E. S. Monuki, *Stem Cells*, 2008, **26**, 656–665.
44 H. B. Li and R. Bashir, in *Biomems and Bionanotechnology*, ed. R. P. Manginell, J. T. Borenstein, L. P. Lee and P. J. Hesketh, 2002, pp. 167–172.
45 C. L. Asbury, A. H. Diercks and G. van den Engh, *Electrophoresis*, 2002, **23**, 2658–2666.
46 J. C. Weaver, in *Methods in Molecular Biology*, Humana Press, Inc., Totowa, NJ, 1995, pp. 3–28.
47 P. Marszalek, D. S. Liu and T. Y. Tsong, *Biophys. J.*, 1990, **58**, 1053–1058.